Human Molecular Genetics, 2009, Vol. 18, No. 9 ***1612–1623***
doi:10.1093/hmg/ddp079
Advance Access published on February 18, 2009

Protein misfolding is the molecular mechanism underlying MCADD identified in newborn screening

Esther M. Maier[1,†], Søren W. Gersting[1,†], Kristina F. Kemter[1], Johanna M. Jank[1], Maria Reindl[1], Dunja D. Messing[1], Marietta S. Truger[1], Christian P. Sommerhoff[2] and Ania C. Muntau[1,*]

[1]Department of Molecular Pediatrics, Children's Research Center, Dr. von Hauner Children's Hospital, Ludwig-Maximilians-University, Lindwurmstr. 4, Munich 80337, Germany and [2]Department of Clinical Chemistry and Clinical Biochemistry, Ludwig-Maximilians-University, Munich 80336, Germany

Received January 13, 2009; Revised and Accepted February 16, 2009

Newborn screening (NBS) for medium-chain acyl-CoA dehydrogenase deficiency (MCADD) revealed a higher birth prevalence and genotypic variability than previously estimated, including numerous novel missense mutations in the *ACADM* gene. On average, these mutations are associated with milder biochemical phenotypes raising the question about their pathogenic relevance. In this study, we analyzed the impact of 10 *ACADM* mutations identified in NBS (A27V, Y42H, Y133H, R181C, R223G, D241G, K304E, R309K, I331T and R388S) on conformation, stability and enzyme kinetics of the corresponding proteins. Partial to total rescue of aggregation by co-overexpression of GroESL indicated protein misfolding. This was confirmed by accelerated thermal unfolding in all variants, as well as decreased proteolytic stability and accelerated thermal inactivation in most variants. Catalytic function varied from high residual activity to markedly decreased activity or substrate affinity. Mutations mapping to the β-domain of the protein predisposed to severe destabilization. *In silico* structural analyses of the affected amino acid residues revealed involvement in functionally relevant networks. Taken together, our results substantiate the hypothesis of protein misfolding with loss-of-function being the common molecular basis in MCADD. Moreover, considerable structural alterations in all analyzed variants do not support the view that novel mutations found in NBS bear a lower risk of metabolic decompensation than that associated with mutations detected in clinically ascertained patients. Finally, the detailed insight into how *ACADM* missense mutations induce loss of MCAD function may provide guidance for risk assessment and counseling of patients, and in future may assist delineation of novel pharmacological strategies.

INTRODUCTION

Newborn screening (NBS) for medium-chain acyl-CoA dehydrogenase deficiency (MCADD; MIM #201450) by tandem-mass spectrometry has successfully been implemented in many countries worldwide (1). MCADD revealed a notably higher birth prevalence (∼1:15000) than previously estimated (1–3) and nowadays is the disorder most frequently diagnosed in NBS, together with phenylketonuria (4). The disease leads to a defect in mitochondrial β-oxidation of fatty acids. Patients show a decreased ability to withstand catabolic stress and risk coma and death due to hypoketotic hypoglycemia during prolonged fasting or intercurrent illness. In undiagnosed patients, the disorder shows a significant morbidity and mortality. Approximately 20% of patients die during their first metabolic crisis and ∼40% of the survivors show sustained neurological impairment (5–7). Once diagnosed, however, adverse effects can be prevented by avoidance of fasting during episodes of catabolic stress. Thus, MCADD is the disorder thought to most justify early detection by NBS (4).

In patients diagnosed after metabolic decompensation, the mutation K304E (c.985A>G) (*ACADM* gene; OMIM #607008) has been shown to account for 90% of defective alleles (8) and therefore is considered to be a severe mutation associated with a high risk of clinical manifestation (9).

*To whom correspondence should be addressed. Tel: +49 89 5160 2746; Fax: +49 89 5160 7792; Email: ania.muntau@med.uni-muenchen.de
†The authors wish it to be known that, in their opinion, the first two authors should be regarded as joint First Authors.

K304E and few other missense mutations identified in symptomatic patients were previously shown to induce protein misfolding and aggregation (10–17).

MCADD patients identified by NBS show a considerably wider genotypic heterogeneity with the mutation K304E being less prevalent. Numerous novel mutations were unraveled including a second prevalent mutation, Y42H (c.199T>C) (3,18–20). After diagnosis, patients carrying these allelic variants follow disease management plans to avoid metabolic crises. Thus, the natural course of MCADD associated with this new group of mutations is unlikely to be witnessed. On average, these patients express lower disease markers (octanoylcarnitine and related acylcarnitine ratios in blood) than observed in homo- or heterozygosity for K304E (3,18,20). However, the different genotypes show a high variability of values, and it is generally accepted that the biochemical phenotype does not allow for a reliable assessment of the risk associated with the single mutations. Insights into the molecular effects of the mutations on the corresponding protein would be helpful to estimate their pathogenic relevance. Yet, experimental data on the molecular consequences of the various novel missense mutations identified in NBS is scarce and mainly refers to the mild temperature-sensitive Y42H mutation (18,21,22). The aim of this study, therefore, was to elucidate the impact of mutations found in presymptomatic newborns on conformation, stability and catalytic function of the variant MCAD proteins.

MCAD is a member of the acyl-CoA dehydrogenase (ACAD) family of flavoproteins, which catalyzes the first step of the mitochondrial β-oxidation of medium-chain fatty acids. The ACAD family comprises nine known members, five of which are involved in fatty acid oxidation, four in amino acid oxidation (23). Each subunit of the homotetrameric MCAD enzyme is composed of three structural domains of approximately equal size, namely the N-terminal α-domain (residues 1–129), the β-domain (residues 130–239) and the C-terminal α-domain (residues 240–396). The N- and C-terminal domains predominantly consist of densely packed α-helices, which shape the core of the tetramer. The middle β-domains are exposed at the surface of the molecule and comprise two orthogonal β-sheets. The catalytic centers consisting of the binding sites for the substrate and the natural cofactor flavin adenine dinucleotide (FAD) are mainly formed by the interface between the β-domain and the C-terminal α-domain. The three-dimensional (3D) structure is a tetrahedral arrangement of a dimer of dimers with an overall diameter of ∼90Å. The interactions between the two monomers forming a dimer are extensive and involve the FAD binding site, whereas between the two dimers predominantly helix–helix interactions are found, similar to a four-helix bundle structure (23).

In this study, we characterized ten MCAD variants with single amino acid substitutions spread over the protein derived from mutations previously reported from the NBS in Bavaria, Germany, including the two prevalent mutations Y42H and K304E (3). We established a high-yield purification protocol for recombinant prokaryotic expression of wild-type and variant MCAD proteins using a maltose binding protein (MBP)-tag. The purified proteins were subsequently characterized with respect to oligomerization, enzyme kinetics, proteolytic stability, thermal inactivation and thermal unfolding. Impressively, all variants showed alterations of protein function, yet in heterogeneous ways. Catalytic function varied from high residual activity to markedly decreased activity and severe alteration of substrate affinity. We observed aggregation with partial rescue by co-overexpression of chaperonins, decreased proteolytic stability and accelerated thermal inactivation in most variants. Thermal unfolding was facilitated in all variants. Data on proteolytic and thermal stability revealed that conformational changes and destabilization are most pronounced in mutations mapping to the β-domain of the protein. These results substantiate the hypothesis of protein misfolding with loss-of-function being the common molecular basis in MCADD. The hypothesis holds true not only for the common variant K304E, but also for mutations derived from presymptomatic patients.

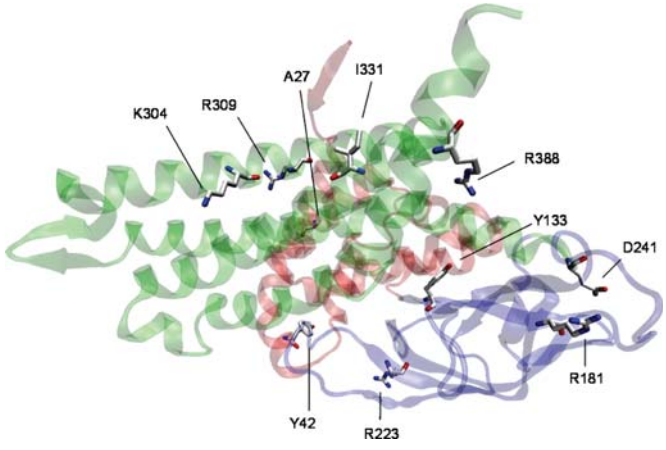

Figure 1. Structural localization of *MCAD* missense mutations analyzed. The MCAD monomer, shown as a ribbon representation, is composed of three structural domains: the N-terminal α-helix domain (residues 1–129, red), the β-sheet domain (residues 130–239, blue) and the C-terminal α-helix domain (residues 240–396, green). Amino acid residues affected by mutations are shown as stick models with carbon atoms in white, oxygen atoms in red and nitrogen atoms in blue.

RESULTS

Disturbed oligomerization is partially rescued by co-overexpression of GroESL

Wild-type and ten variant forms of MCAD (Fig. 1 and Table 1) were purified by affinity chromatography and subsequent size-exclusion chromatography (SEC) to analyze the oligomeric states of the expressed fusion proteins (Fig. 2). Wild-type MCAD was eluted in the tetrameric form with an almost negligible amount of aggregates (<1%), whereas MCAD variants showed a markedly decreased expression of soluble protein consistent with proneness to aggregation and degradation of misfolded protein. Only one variant (R388S) showed an elution profile identical to wild-type. The remaining variants revealed severely disturbed oligomerization consisting of (i) small amounts of tetramers (Y42H, D241G, R309K) with or without high molecular weight aggregates, (ii) exclusively high molecular weight aggregates (A27V, K304E, I331T) or (iii) small amounts of protein fragments of various molecular weights (Y133H, R181C) (Fig. 2A). No monomers or dimers were observed with any of the variants. R223G was expressed

Table 1. cDNA and protein location of MCAD missense mutations analyzed

cDNA[a]	Mature protein
c.155C>T	A27V
c.199T>C	Y42H
c.472T>C	Y133H
c.616C>T	R181C
c.742A>G	R223G
c.797A>G	D241G
c.985A>G	K304E
c.1001G>A	R309K
c.1067T>C	I331T
c.1237C>A	R388S

[a]Reference sequence: GenBank accession no. M16827.1. Nucleotide numbering starts with A of the ATG initiation codon as +1.

as truncated, instable protein with no detectable activity (data not shown) and could not be subjected to SEC.

Tetramer formation was partially rescued by co-overexpression of the chaperonins GroES and GroEL. Co-overexpressing GroESL, seven variants (A27V, Y42H, Y133H, R181C, D241G, K304E, R309K) showed oligomerization profiles similar to that of wild-type with only small amounts of aggregates (5–7%) (Fig. 2B). Co-overexpression of chaperonins did not enhance protein folding for the two variants I331T and R223G.

In summary, we observed disturbed oligomerization with aggregation and/or degradation in nine of 10 MCAD variants analyzed. Our results confirm that *ACADM* mutations can compromise protein folding, but misfolding can be mitigated to various extent by increasing the amount of available chaperonins.

Variant MCAD proteins show different patterns of enzyme kinetic parameters

Kinetic analyses using the ferricenium ion as an electron acceptor were performed for wild-type and purified MCAD variants (Table 2). All variants displayed Michaelis–Menten behavior. Enzyme activity with respect to V_{max} was comparable to wild-type in variants Y42H, R181C and R309K. Reduced maximal activities were found in variants A27V (38% of wild-type), D241G (48%) and K304E (46%). Variant Y133H showed the most pronounced reduction in activity (3.5%), but still followed Michaelis–Menten kinetics. V_{max} of wild-type, Y42H, and K304E are in line with the previously reported data (14,21,24).

For most of the variants, the apparent affinity to the substrate octanoyl-CoA was not or only slightly reduced. Only R388S showed an excessively decreased substrate affinity with a 100-fold increase in K_m (51.9 μM). This variant showed a 2.5-fold increase in V_{max}. However, the apparently high activity is of no physiological relevance, since it would require supraphysiological concentrations of substrate to achieve it.

K_m-values displayed in this study are 10-fold lower compared with previously reported data (14,21,24). This

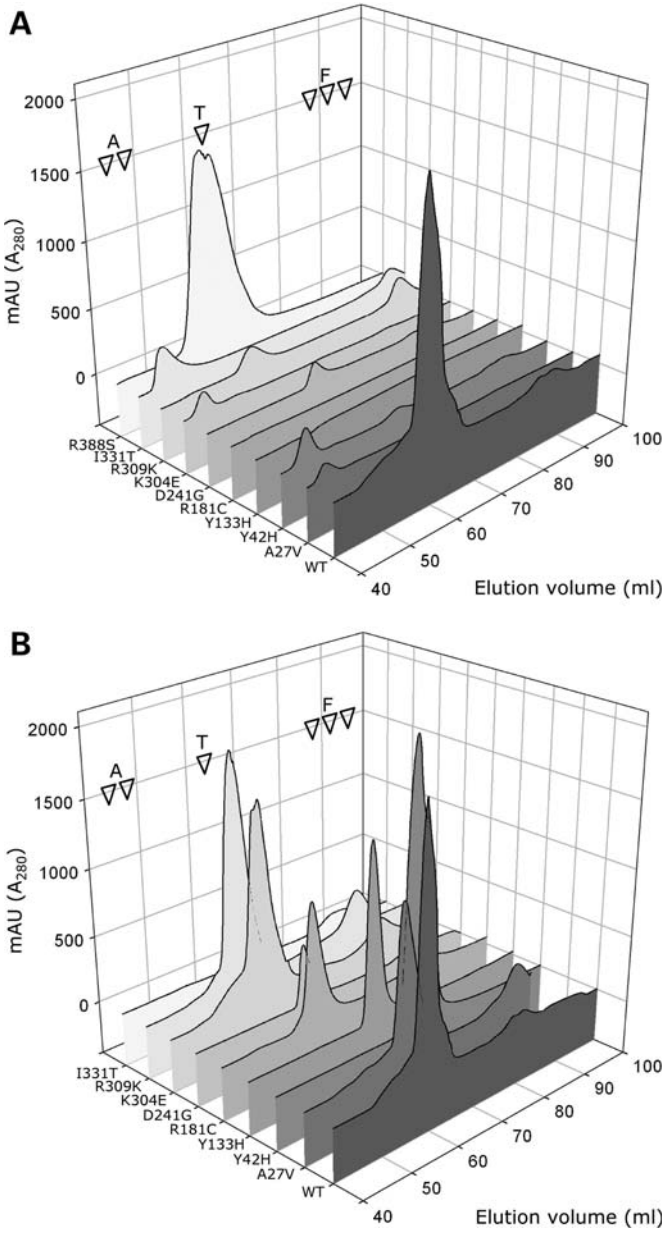

Figure 2. Disturbed oligomerization of variant MCAD proteins is partially rescued by co-overexpression of GroESL. Oligomerization profiles of wild-type (WT) and variant MCAD proteins were determined by size-exclusion chromatography. Soluble high molecular weight aggregates (A) eluted at volumes of 45–47 ml, tetramers (T) at 58–62 ml. No dimers or monomers were observed with any of the variants. Elution volumes of >85 ml contained fragments (F) of degraded MCAD or MBP. (**A**) Profiles without co-overexpression of GroESL. Wild-type (WT) and R388S almost exclusively eluted as tetramers. All other variants eluted as high molecular weight aggregates or low molecular weight fragments with only three variants (Y42H, D241G and R309K) showing small peaks of tetrameric MCAD. Aggregates and degradation products of Y133H and R181C comprised various molecular weights spread all over the chromatogram. (**B**) Profiles with co-overexpression of GroESL. Variants A27V, Y42H, Y133H, R181C, D241G, K304E and R309K showed a rescue of tetramer formation with only small amounts of aggregates. Only for variant I331T, tetramer formation could not be restored. Note: for WT, the chromatogram without co-overexpression of GroESL is depicted.

Table 2. Enzyme kinetic parameters of wild-type and variant MCAD proteins

Missense mutation	K_m (μM octanoyl-CoA)	SEM[b]	V_{max} (μmol ferricenium/min × mg protein)	SEM[b]
WT	0.4	0.04	37.1	1.49
A27V	0.5	0.11	14.1	1.16
Y42H	0.7	0.10	35.4	3.00
Y133H	0.7	0.11	1.3	0.13
R181C	0.9	0.11	41.5	0.77
D241G	0.8	0.23	17.7	1.43
K304E	0.6	0.29	17.0	2.08
R309K	0.7	0.11	32.0	0.92
R388S[a]	51.9	12.67	88.2	13.54

Steady-state kinetic parameters of wild-type (WT) and variant tetrameric MCAD proteins. Maximum activities (V_{max}) and apparent substrate affinities (K_m) of octanoyl-CoA oxidation were determined by Michaelis–Menten kinetics using a substrate range of 0–20 μM.
[a]Enzyme kinetic parameters determined at 0–150 μM octanoyl-CoA.
[b]Standard error of the mean of $n = 3$ independent experiments.

Table 3. Proteolytic stability of wild-type and variant MCAD proteins

Missense mutation	$t_{1/2}$ (min)	SEM	*P*-value	Plateau (%)	SEM	*P*-value
WT	31.2	6.6		70.1	5.8	
A27V	34.5	2.8	ns	57.6	3.7	ns
Y42H	41.2	4.0	ns	56.8	10.6	ns
Y133H	7.2	0.2	<0.05	10.0	3.6	<0.01
R181C	29.4	8.7	ns	33.4	6.0	<0.01
D241G	23.9	3.8	ns	8.2	2.5	<0.01
K304E	30.7	7.3	ns	61.6	5.0	ns
R309K	7.7	2.7	<0.05	47.6	1.9	<0.01
R388S	19.2	7.30	ns	52.3	1.2	ns

Stability of wild-type (WT) and variant MCAD proteins against limited proteolysis by proteinase K. The velocity of degradation ($t_{1/2}$) was assessed using a low protease:substrate ratio (1:25). The amount of protein not susceptible to proteolysis (plateau) was determined at a higher protease:substrate ratio (1:1). The calculated half-lives ($t_{1/2}$) are given in minutes, plateaus of degradation in per cent, both with corresponding standard errors of the mean (SEM) of $n = 3$ independent experiments. Significances for the differences between wild-type and the variants were calculated by one-way ANOVA and a Dunnett's post test. (ns, not significant).

observation might be an effect of correcting our measurements for background ferricenium reduction, correcting octanoyl-CoA concentrations for oxidizable substrate (see Materials and Methods) and optimizing the assay for sensitive and short duration measurements. However, the scale of the reported differences between K_m-values of wild-type, Y42H and K304E is well comparable.

Taken together, the MCAD variants analyzed showed different patterns of kinetic parameters: (i) activity comparable to wild-type, (ii) reduced and markedly reduced maximal activity and (iii) an excessive decrease in affinity to octanoyl-CoA as a substrate.

Susceptibility to proteinase K is increased

Limited proteolysis is used for probing protein conformation and folding kinetics. It can provide important information on local unfolding and the equilibrium between the native state oligomeric protein and its folding intermediates, since misfolded proteins are more susceptible to degradation by proteases (25). To this aim, MCAD proteins were probed with proteinase K, because its proteolysis is not limited to sequence specificity but by stereochemistry and flexibility of the protein substrate. The proteolytic stability of wild-type and variant MCAD proteins was analyzed by determination of the half-lives, indicating the velocity of degradation, and the plateaus of degradation, indicating the residual amount of protein not susceptible to proteolysis (Table 3). Five variants (Y133H, R181C, D241G, R309K and R388S) showed reduced half-lives compared to wild-type, two of which reached statistical significance (Y133H and R309K). The plateaus of degradation, however, were significantly decreased in 4 of these variants (Y133H, R181C, D241G and R309K). This finding was most pronounced in variants Y133H and D241G with residual protein amounts of 10 and 8%, respectively. Notably, the plateau of degradation of the wild-type protein was found to be 70%, indicating that at the assay conditions (37°C, 120 min) 30% of the wild-type protein is unfolded. This finding reflects the thermal sensitivity of the MCAD protein, which is additionally influenced by the protein concentrations used in the assay (21).

The decreased proteolytic stability of the variants compared to wild-type is in line with the hypothesis of an altered folding equilibrium shifted towards folding intermediates and destabilization due to local protein unfolding.

Resistance of catalytic function against thermal stress is reduced

We assessed the thermal effect on activity of wild-type and variant MCAD proteins over a range of 25–55°C. The midpoint of thermal inactivation ($T_{1/2}$), i.e. the temperature at 50% residual activity, was monitored by determination of the residual activity at different temperatures. Near the midpoint of denaturation of the wild-type (44.5°C), kinetic stability expressed as half-lives ($t_{1/2}$) was determined at 41°C (Fig. 3 and Table 4). A significant reduction of $T_{1/2}$ compared with wild-type was found in all MCAD variants analyzed except for K304E and R388S. Alterations were most pronounced in Y133H (33.6°C), R181C (34.3°C) and D241G (33.9°C). These three variants also showed significantly decreased half-lives of 6.1 min (Y133H), 6.8 min (R181C) and 9.7 min (D241G) when subjected to thermal stress as a function of time (wild-type 20.0 min). The differences among wild-type, Y42H and K304E with respect to $T_{1/2}$ are in line with the previously published data (14,18,21,26).

These observations indicate that temperature has a significant impact on catalytic function in variant MCAD proteins. Notably, these effects are detectable at physiologically relevant temperatures.

Thermal stress induces accelerated denaturation

To determine aberrant folding of MCAD with respect to ground state hydrophobicity and thermal denaturation, we performed 8-anilino-1-naphtalenesulfonic acid (ANS)

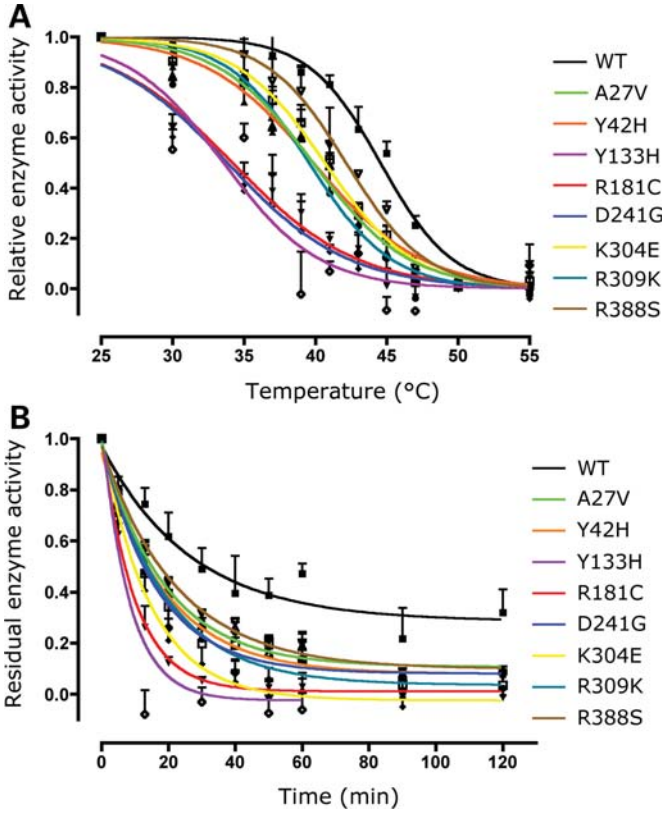

Figure 3. Variant MCAD proteins show early thermal inactivation and reduced kinetic stability. The effect of thermal stress on enzyme activity of wild-type (WT) and variant MCAD was analyzed. (**A**) Thermal inactivation profiles. Proteins were incubated at increasing temperatures (25–55°C) and the residual enzyme activities were determined. All variants showed a left-shift of the curves in comparison to WT indicating an inactivation of the enzyme at lower temperatures (Table 4, left panel). (**B**) Kinetic stability at 41°C. Proteins were incubated at 41°C and the residual enzyme activity was determined at incremental time points. For all variants, steeper slopes of the curves were observed indicating a reduction of half-lives compared with WT (Table 4, right panel). Data points of residual activities in both datasets were normalized to the initial enzyme activity and subjected to non-linear regression analysis. Error bars represent the mean ± SEM of $n = 3$ independent experiments.

Table 4. Thermal inactivation and kinetic stability of wild-type and variant MCAD proteins

Missense mutation	Thermal inactivation			Kinetic stability at 41°C		
	$T_{1/2}$ (°C)	SEM	*P*-value	$t_{1/2}$ (min)	SEM	*P*-value
WT	44.5	0.45		20.0	2.36	
A27V	39.8	0.88	<0.05	11.8	2.28	ns
Y42H	39.8	0.52	<0.05	12.7	1.35	ns
Y133H	33.6	1.01	<0.01	6.1	1.14	<0.01
R181C	34.3	1.28	<0.01	6.8	0.88	<0.01
D241G	33.9	1.08	<0.01	9.7	0.91	<0.05
K304E	40.6	0.43	ns	12.8	2.53	ns
R309K	38.8	1.80	<0.01	12.9	1.57	ns
R388S	42.0	0.37	ns	15.7	0.59	ns

Thermal inactivation and kinetic stability of wild-type (WT) MCAD were compared with variant MCAD proteins. For thermal inactivation, residual activities at different temperatures (25–55°C) were subjected to non-linear regression analysis and the midpoints of thermal inactivation ($T_{1/2}$) were calculated. $T_{1/2}$-values represent the temperature at 50% residual activity and are given in degree Celsius as means with the corresponding standard errors of the mean (SEM) of $n = 3$ independent experiments. For kinetic stability, the inactivation at 41°C was determined as a function of time. The residual activities were subjected to non-linear regression analysis and the half-lives ($t_{1/2}$) were calculated. $t_{1/2}$-values represent the time point at 50% residual activity and are given in minutes as means with the corresponding standard errors of the mean (SEM) of at least $n = 3$ independent experiments. Significances for the differences between wild-type and the variants were calculated by one-way ANOVA and a Dunnett's post test. (ns, not significant).

fluorescence experiments. The use of the hydrophobic fluorophore ANS allowed monitoring of overall unfolding events, since it binds to hydrophobic groups of the denaturing protein showing a high quantum yield in its bound state, but not when solved in aqueous buffers (27). ANS fluorescence analysis of tetrameric wild-type MCAD revealed a transition midpoint ($T_{m1/2}$) between folded and unfolded state of 52.6°C. This is in agreement with previous results obtained by circular dichroism (16).

Figure 4A shows ANS fluorescence profiles upon thermal denaturation of wild-type, K304E and two severely distorted variants. In variant Y133H, a considerably (20-fold) elevated ground state fluorescence signal at 25°C was detected in comparison with wild-type. This finding indicates an increased hydrophobicity due to partial protein unfolding even without the application of thermal stress. The same was found in R181C and K304E, but to a much lesser extent. Upon thermal denaturation, for all MCAD variants the transition from the native state to the unfolded state occurred at significantly lower temperatures than in the wild-type (Fig. 4B and Table 5). The variants Y133H and R181C showed the most pronounced alterations with $T_{m1/2}$ of 42.2 and 40.0°C, respectively. In addition to the marked left-shift of the curve, Y133H revealed a steeper slope of the curve indicating an accelerated progress of unfolding with complete denaturation at 46°C.

In summary, we observed facilitated unfolding upon thermal stress of various degrees in all variants, but also partial unfolding/misfolding in the ground state for some variants. The variant Y133H disclosed signs of severe impairment of structural integrity consistent with the findings from the other stability experiments.

Functional and conformational impact of amino acid replacements on 3D networks of side-chain interactions

Our experiments revealed severe functional and structural impairment, in particular, for the variants Y133H, R181C and R388S. To gain further insights into how these mutations exert their deleterious effects on the protein, we used a 3D structural model of the porcine MCAD tetramer to investigate, whether the amino acid residues affected are involved in networks of side-chain interactions with functional and conformational impact.

Residue Y133 maps to the β-sheet domain (residues 130–239) and is an essential part of the active site (Fig. 5A). It directly interacts with the cofactor FAD via hydrogen bond formation. Its aromatic side-chain points towards the hydrophobic core of the deep binding cavity for the fatty acid portion of the substrate establishing hydrophobic interactions with the residues L103, V135, F177, A248 and F252 which

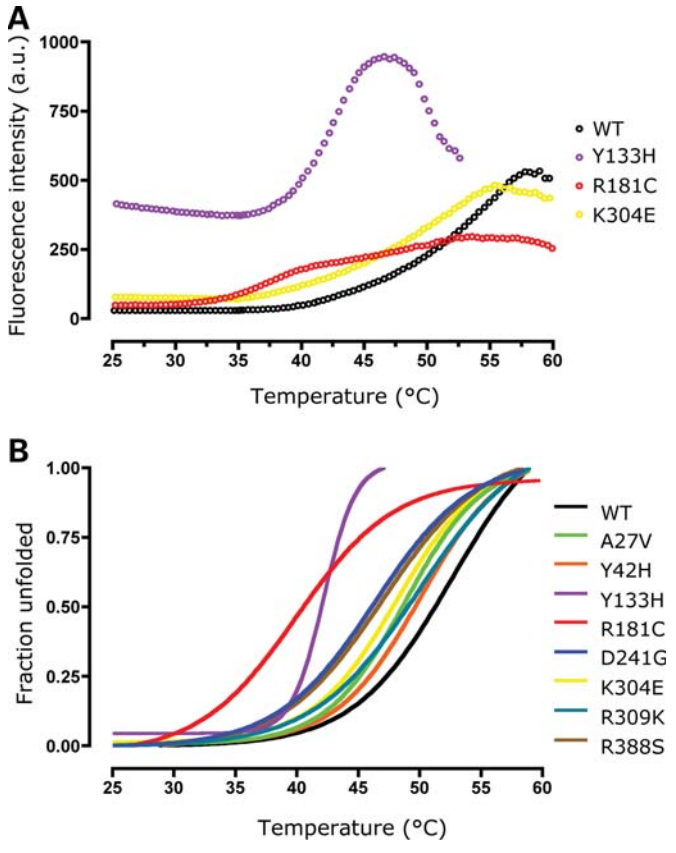

Figure 4. Variant MCAD proteins show accelerated thermal denaturation and partial protein unfolding in the ground state for some variants. Thermal unfolding of wild-type (WT) and variants monitored by ANS fluorescence. (**A**) ANS fluorescence profiles of wild-type, Y133H, R181S and K304E. Intensities of the fluorescent dye ANS, which binds to hydrophobic groups of the protein presented upon unfolding, are plotted as a function of increasing temperatures. Ground-state fluorescence was markedly increased for Y133H and, to a lesser extent, for R181C and K304E indicating an increased hydrophobicity due to partial unfolding of these variants already in the native state. (**B**) Thermal denaturation of all variants analyzed. Fractions of unfolded protein are plotted as a function of increasing temperatures and the transition midpoints represent the temperature at half denaturation (fraction unfolded 0.5). All variants showed a marked to moderate left-shift of the curves implying an increased propensity to unfold upon thermal stress (Table 5). In addition, Y133H showed accelerated unfolding as indicated by the steeper slope of the curve and complete denaturation at 46°C.

line the cavity. To poise the $C_\alpha - C_\beta$ bond of the fatty acid for dehydrogenation, it is sandwiched between the *re*-face of the isoalloxazine moiety of FAD and the catalytic base E376. A replacement of the large, hydrophobic tyrosine by the smaller, positively charged histidine is supposed to distort the hydrophobic packing of the binding cavity and by this to lead to a conformational rearrangement of the active site pocket. As a result, the correct 3D arrangement of FAD, the $C_\alpha - C_\beta$ bond of the substrate and the catalytic base E376 will be impaired leading to the marked disturbance in enzyme function. Moreover, A248 and F252 are located within the α-helix G. Interactions between α-helices G and H in one subunit of the dimer and α-helices I and K in the opposite unit of the adjacent dimer are known to promote MCAD tetramer assembly from dimers. Hence, conformational alteration of the substrate binding cavity with impairment of the helix–helix interactions due to the Y133H substitution might explain the observed distortion of the oligomeric state.

Table 5. Transition midpoints of thermal denaturation of wild-type and variant MCAD proteins

Missense mutation	$T_{m1/2}$ (°C)	SEM	*P*-value
WT	52.6	0.40	
A27V	48.8	0.69	<0.01
Y42H	50.1	0.19	<0.01
Y133H	42.2	0.11	<0.01
R181C	40.0	0.16	<0.01
D241G	46.4	0.65	<0.01
K304E	48.2	0.16	<0.01
R309K	50.0	0.14	<0.01
R388S	47.0	0.85	<0.01

Transition midpoints of thermal denaturation obtained by ANS fluorescence of wild-type (WT) MCAD were compared with variant proteins. Three sets of independent experiments were performed. The transition midpoints ($T_{m1/2}$) were calculated by non-linear regression analysis and are given in degree Celsius as means with their corresponding standard errors of the mean (SEM). Significances for the differences between wild-type and variants were calculated using one-way ANOVA followed by a Dunnett's post test.

R181 is located at the beginning of an extended loop structure (residues 181–193) at the surface of the protein that connects β-sheets 4 and 5 (Fig. 5B). The loop contributes to the crevice shaping the entrance to the active site and, due to its strong interactions with the beginning of the C-terminal α-domain, plays a pivotal role for MCAD tetramerization. R181 networks with D183, D185, K187 and A188 to poise the loop in its proper structural conformation. It is well conceivable that the severe structural distortion of the protein with reduced stability and impaired tetramer assembly shown for R181C is due to a disruption of this network caused by the replacement of arginine by a small, polar, uncharged amino acid.

R388 maps to the end of the C-terminal α-domain (residues 240–396) and is part of an interface of two subunits that define a funnel-shaped crevice, the entrance to the active site mentioned above (Fig. 5C). It is shaped by α-helix K and the loops among β-sheets 4 and 5, α-helices H and I and α-helices G and H of the adjacent subunit. R388 forms a hydrogen bond to the AMP portion of the CoA moiety and is part of a side-chain network comprising both hydrogen bonds and electrostatic interactions with the neighboring residues E389 and R324 in the loop between α-helices H and I. A substitution of the large, basic, positively charged arginine by serine might disrupt this network by introducing a gap in the 3D structure of the crevice. This conformational rearrangement at the entrance to the active site will hinder the accessibility of the substrate octanoyl-CoA and the interaction with the AMP portion of the CoA moiety. This is in line with our observation that R388S displays a significant decrease in substrate affinity for octanoyl-CoA.

DISCUSSION

NBS for MCADD has revealed an increasing number of missense mutations that have never been identified in clinically diagnosed patients and we have previously described eight

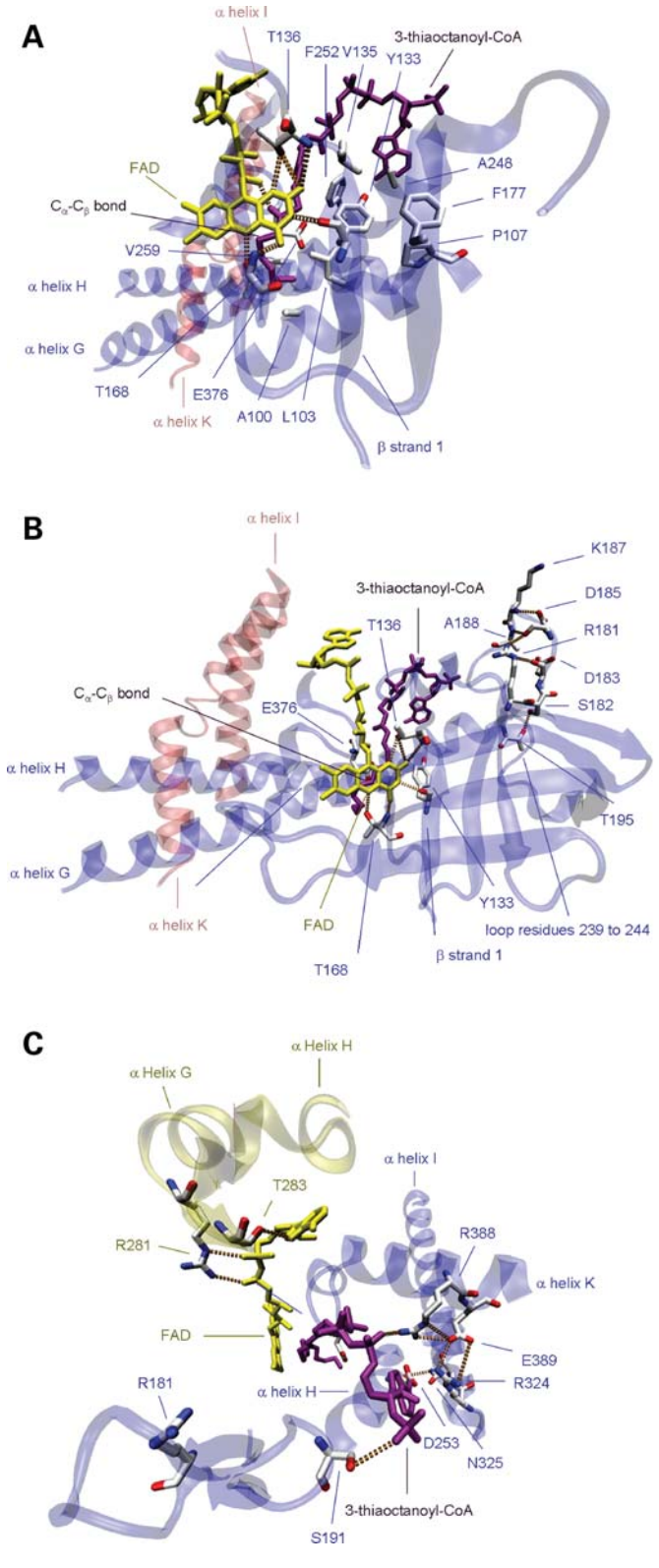

Figure 5. Functional and conformational involvement of amino acid residues affected by *MCAD* mutations in networks of side-chain interactions. Selected parts of subunit backbones are shown as ribbon representations. Selected residues are depicted as stick models with carbon atoms in white, oxygen atoms in red and nitrogen atoms in blue. Hydrogen bonds and electrostatic interactions are shown as golden dotted lines. The cofactor FAD and the substrate analog 3-thiaoctanoyl-CoA are shown in yellow and in purple, respectively. (**A**) Residue Y133 is located at the beginning of the β-domain of the protein (subunit A, blue). It is part of the active site crevice by binding the isoalloxazine ring of FAD, together with T136 and T168. The aromatic side chain of Y133 establishes hydrophobic interactions with A100, L103, P107, V135, F177, A248, F252 and V259. These residues shape the hydrophobic core of the deep binding cavity for the fatty acid portion of the substrate. The precise three-dimensional arrangement of FAD, the C_α–C_β bond of the substrate and the catalytic base E376 is the basis for enzyme function. Moreover, the structural integrity of the hydrophobic core of this cavity is crucial for the assembly of tetramers from dimers by four-helix bundle interactions between α-helices G and H in one subunit (subunit A, blue) and α helices I and K in the opposite unit of the adjacent dimer (subunit D, red). (**B**) The guanidinium side-chain of R181 adopts a central position in the extended loop structure (residues 182–193) at the surface of the protein that connects β-strands 4 and 5 (subunit A, blue). R181 networks with loop residues D183, D185, K187 and A188 via hydrogen bonds, and this contributes to the correct spatial conformation of the loop. The neighboring S182 interacts with T195 in β-strand 5, which establishes interactions to the loop (residues 239–244) interconnecting the β-domain with the C-terminal α-domain. The following α-helix G is part of both the hydrophobic core of the active site and the four-helix bundle between α-helices G and H in one subunit (subunit A, blue) and α-helices I and K in the opposite unit of the adjacent dimer (subunit D, red) assembling the tetramer. The active site is represented by the cofactor FAD interacting with Y133, T136 and T168, the C_α–C_β bond of the substrate, and the catalytic base E376. (**C**) Residue R388 is located in the C-terminal α-helix K and is part of an interface between two subunits forming the dimer (subunit A, blue; subunit B, yellow). The interface defines a funnel-shaped crevice, the entrance to the active site. Subunit A (blue) lines the crevice with α-helix K and the loops between β-strands 4 and 5 (containing R181) and α-helices H and I. The adjacent subunit B (yellow) contributes to the interface via the loop between α-helices G and H. R388 joins a network of hydrogen bonds and electrostatic interactions comprising residues E389, R324, N325, D253 and S191, which bind the CoA moiety of the substrate to the entrance of the active site (subunit A, blue). R281 and T283 in the adjacent subunit (subunit B, yellow) interact with the pyrophosphate and the adenine ring of the cofactor FAD.

of these mutations identified in the Bavarian NBS program (3). Since clinical management protects patients diagnosed by NBS from sequels of catabolic stress, the clinical risk associated with this particular set of mutations still remained unclear. The question, whether patients carrying these mutations might be at lower or no risk of experiencing metabolic decompensation is therefore a matter of controversial debate, and concern has been raised on whether NBS creates unwarranted anxiety in parents and health-care professionals (21,28). To address this issue, we analyzed the corresponding recombinant variant proteins aiming (i) to evaluate whether the mutations are genuinely pathogenic, (ii) to assess the severity of the mutation's impact and (iii) to elucidate the molecular mechanisms of loss-of-function. Having applied complementary strategies, we provide several lines of experimental evidence that all novel missense mutations identified in our NBS lead to protein misfolding with severe impact on structural conformation, protein stability and to a lower extent, on enzyme kinetics. Thus, our results support the hypothesis that MCADD adds to the growing catalogue of protein misfolding disorders with loss-of-function. Moreover, the experimental data do not support the view that novel mutations found in NBS bear a lower risk of metabolic decompensation than that associated with mutations detected in clinically ascertained patients, but this remains a possibility.

Two variants showed a complete loss of protein function due to aggregation (I331T) and degradation (R223G), respectively. Most remaining variants necessitated co-overexpression of GroESL for tetramer assembly. Only R388S formed into

apparently normal tetramers without co-overexpression of chaperonins. The findings of increased propensity of variant MCAD proteins to form aggregates in *Escherichia coli* and partial rescue by increasing the amount of available chaperonins was regarded as a first evidence for misfolding. Although co-overexpression of GroESL can assist to overcome protein misfolding in terms of aggregation and by this promote the formation of correctly assembled oligomers (29), it does not correct for the mutation induced structural defects of the variant protein. These defects were then analyzed in detail in this study.

All purified tetrameric MCAD variants revealed alterations of structural conformation, yet of various degrees. Interestingly, all variants showed thermal instability. Thermal unfolding was accelerated with a shift of the transition midpoint (wild-type, 52.6°C) by >4°C in most variants and down to 40°C in variant R181C. Thermal inactivation experiments revealed a 50% loss-of-function at temperatures <40°C (wild-type 44.5°C) in all variants except for K304E and R388S. This observation is of particular interest, since in a considerable share of patients with MCADD metabolic decompensation occurs during intercurrent illness with fever. These findings are in line with the previous data on thermal stability of other variant MCAD proteins (14–16,21,22). Moreover, we observed that thermal instability was most pronounced in variants mapping to the β-sheet domain of the protein (Y133H, R181C) or to the loop interconnecting this domain and the C-terminal α-helix domain (D241G).

Additional evidence for protein instability arose from our data on limited proteolysis. Most variants showed an increased susceptibility against proteolytic attack indicating disturbed folding kinetics (i.e. shift of the folding equilibrium towards the unfolded state) and local unfolding. Mild alterations were observed in variants derived from mutations located in the tightly packed C-terminal α-domain. Again, the variants mapping to the β-sheet domain and its subsequent loop disclosed the most pronounced alterations consistent with severe conformational changes.

In two variants located in the β-sheet domain (Y133H and R181C), severe alterations of protein conformation were evident even without thermal or proteolytic stress. Elevated ground state ANS fluorescence revealed an increase in hydrophobicity and thus a shift to the non-native state of these proteins. In Y133H, the induced conformational changes led to a severe destabilization and almost complete loss-of-function with a residual catalytic activity of 3.5%. The affected amino acid residue Y133 is part of the active site in two respects. Together with T136 and T168, it anchors the co-factor FAD to the protein via hydrogen bonds. In addition, the aromatic side chain of Y133 contributes to the hydrophobic core lining the binding cavity for the fatty acid. Previous studies characterizing the molecular phenotype of T168A (c.577A>G), a mutation that has been identified in a clinically diagnosed patient, are in line with our observations revealing misfolding, markedly decreased thermal stability and catalytic activity (15,16,18). In contrast, R181C showed a residual catalytic activity comparable to wild-type despite its severe conformational alterations. Our data are consistent with the notion that the major molecular basis for the pathogenesis of this variant *in vivo* may be protein instability under physiological stress pointing to a high risk of metabolic decompensation during times of illness, especially associated with fever. As previously reported, a patient homozygous for this mutation showed remarkably mild biochemical alterations in NBS (3), although a mutation affecting the same amino acid residue (R181L; c.617G>T) was identified in two symptomatic patients (30). Our experimental data emphasize that mild biochemical alterations in NBS do not allow implying a low risk for decompensation.

Mutations located in the N-terminal α-domain showed moderate effects on tetramer assembly and thermal stability together with decreased (A27V) or normal catalytic activity (Y42H). Consistent with our findings, mutations located in this region have previously been described as mild folding variants with normal activity (M124I; c.447G>A), medium range activity (R28C; c.157C>T) or moderate thermal instability (Y42H) (10,21). However, α-helices A, C and D of this domain form the recognition site of the electron transfer flavoprotein, which is the natural electron acceptor of the MCAD protein and responsible for the electron transfer to the respiratory chain (31). Whether structural changes in this domain result in an alteration of electron transfer rates remains to be elucidated.

In contrast, mutations located in the C-terminal α-domain (K304E, R309K, I331T) often affect helix–helix interactions crucial for tetramer assembly leading to aggregation (10,12,13,22,23). However, when aggregation was overcome by co-overexpression of chaperonins, these variants showed considerable residual activities. Interestingly, R388S, also located in the C-terminal α-domain, was the only variant that did not require co-overexpression of GroESL for tetramer formation and its proteolytic and thermal stabilities were only moderately affected. In this variant, misfolding resulted in a marked decrease of substrate affinity. Similar effects on K_m have been shown for artificial variants of the homologous arginine residue R387 of the ACAD isovaleryl-CoA dehydrogenase (32) and have been predicted from crystal structure analysis for the ACAD glutaryl-CoA dehydrogenase (33). Our data substantiate the essential role of this highly conserved arginine residue for binding of the substrate in ACADs.

The observations obtained from analyzing variants harboring amino acid substitutions in different regions of the protein show that mutations in the β-sheet domain and the adjacent loop (interconnecting the β-domain and the C-terminal α-domain) are particularly instable and prone to severe conformational distortion. This is in line with the previous work describing severely impaired biogenesis and stability for two other variants located in the β-domain, T168A and G170R (c.583G>A) (10,15). Misfolding observed in these variants has been attributed to the loss of FAD anchoring, which has been reported to be crucial for folding and oligomerization (34). However, the compiled data including our variants spread over the β-domain indicate that not only reduced FAD binding, but also the structural and functional characteristics of the β-domain itself account for the protein destabilization observed.

In conclusion, all mutations analyzed in this study showed significant alterations of the molecular phenotype ranging from mild to severe. Six of the mutations (Y133H, R181C, R223G, D241G, I331T and R388S) identified in presympto-

matic newborns revealed even more pronounced perturbances than the variant K304E, which is generally accepted to be associated with a severe molecular and clinical phenotype. It has to be noted, however, that patients homozygous for K304E may experience a healthy life (2) and our findings of a severe molecular phenotype do not unequivocally prove a severe clinical phenotype. Standard diagnostic procedures such as the determination of blood acylcarnitine concentrations do not allow for a meaningful prediction of the clinical course. Hence, compiled knowledge gained by documentation of the clinical and biochemical course of specific genotypes in combination with detailed molecular characterization of the respective variants at the protein level will improve genotype–phenotype correlation. This may assist counseling and risk assessment of MCADD patients identified in NBS programs. In this context, it has also to be taken into account that most patients revealing mutations other than the predominant K304E are compound heterozygous. Moreover, gene–gene interactions and gene–environment interactions such as cellular and environmental conditions or stressors may also modify the natural course of the disease (35).

A molecular scenario similar to that now identified for MCADD was recently described for the phenylalanine hydroxylase protein, the enzyme deficient in phenylketonuria (36). In this disease, experimental evidence is now available that the well proven efficacy of tetrahydrobiopterin (37,38) is based on a pharmacological chaperone effect. For MCAD, we and others showed that increasing the amount of available molecular chaperones (GroESL) prevents MCAD aggregation and leads to higher amounts of functional protein. The persisting loss-of-function is then predominantly promoted by instability against thermal or proteolytic stress. Early degradation could thus be overcome using pharmacological chaperones, conceivably in combination with proteostasis regulators as recently shown for lysosomal storage diseases (39).

In summary, the detailed insight into how *ACADM* missense mutations induce conformational alteration and protein destabilization resulting in loss of enzyme function presented here may in future provide the basis to delineate novel pharmacological strategies for the potentially fatal MCADD disease.

MATERIALS AND METHODS

Subjects and mutations

In the previous study, we described the spectrum of sequence variations occurring in newborns with MCADD detected by NBS (3). We identified eight novel missense mutations within the *ACADM* gene that have not yet been characterized *in vitro*: A27V (c.155C>T), Y133H (c.472T>C), R181C (c.616C>T), R223G (c.742A>G), D241G (c.797A>G), R309K (c.1001G>A), I331T (c.1067T>C) and R388S (c.1237C>A) (Table 1). Two mutations (R181C and R223G) were found in a homozygous state. The two individuals homozygous for R223G displayed markedly elevated biochemical markers, whereas the individual homozygous for R181C showed only mild alterations. The remaining mutations were found in a compound heterozygous state with the two most prevalent mutations Y42H (c.199T>C) and K304E (c.985A>G). Mutations and biochemical phenotypes of the patients are summarized in Supplementary Material, Table S1. The structural localization of mutations characterized in this study was mapped to the 3D model of the porcine MCAD monomer (Fig. 1).

Plasmid construction and site-directed mutagenesis

The cDNA of human *ACADM* gene (*ACADM*-encoding pKK223 plasmid obtained as a generous gift from Jerry Vockley, Pittsburgh, USA) was cloned into the pMAL-c2X expression vector (New England Biolabs) encoding a N-terminal MBP-tag and a factor Xa cleavage site. *ACADM* mutations were introduced using the PCR-based QuikChange Site-Directed Mutagenesis Kit (Stratagene). After mutagenesis, all expression vectors were verified by DNA sequencing.

Expression and purification

The expression plasmids were used to transform *E.coli* strain BL21-CodonPlus (Stratagene). Bacteria were grown in 2 l of dYT medium (16 g/l tryptone, 10 g/l yeast extract and 5 g/l NaCl) containing 100 μg/ml Ampicillin to OD_{600} 0.6–0.8 at 37°C. Overexpression of wild-type and variant MBP–MCAD fusion proteins was induced with 0.01 mM isopropylthio-β-*D*-galactoside and performed at a reduced growth temperature of 28°C for 20 h. Bacteria were harvested by centrifugation and lysed by sonication. Protein purification was performed using ÄKTApurifier and ÄKTAprime systems (GE Healthcare) at 4°C. The crude extract/protein sample was loaded on a MBPTrap affinity chromatography column (GE Healthcare) equilibrated with column buffer (20 mM Tris–HCl pH 7.4, 200 mM NaCl, 1 mM EDTA, 1 mM DTT) and eluted with the same buffer containing 10 mM maltose after washing out unbound bacterial protein. The eluted protein fractions were pooled and subjected to SEC using a HiLoad 16/60 Superdex 200 column (GE Healthcare) equilibrated with 20 mM HEPES pH 7.0 containing 200 mM NaCl. The fractions containing tetrameric fusion proteins were pooled and incubated for 12 h at 4°C with factor Xa (Novagen) to cleave the MBP-tag of the fusion proteins at a protease to fusion protein ratio (U:μg) of 1:20. Final purification of the cleaved tetrameric MCAD protein was obtained by SEC on a HiLoad 16/60 Superdex 200 column (GE Healthcare) equilibrated with 20 mM HEPES pH 7.0 containing 200 mM NaCl and reached a purity of >98% SDS/PAGE analysis.

Protein concentrations were determined spectrophotometrically using the absorption coefficients at A_{272} and A_{448} (14), or the fluorescent dye binding Quant-iT assay (Invitrogen). Using this approach, up to 14 mg of cleaved MCAD tetrameric protein of high purity (>97%) were obtained from 2 l culture. A summary of the purification protocol is given in Supplementary Material, Table S2.

Co-overexpression of chaperonins GroESL

The respective pMAL-c2X MCAD expression plasmids were co-transformed with pGroESL encoding the proteins GroES and GroEL (40) in *E.coli* strain DH5α (Invitrogen). Growth of bacteria, expression and purification of proteins were performed as described above except for the addition of two

antibiotics, ampicillin (100 μg/ml) and chloramphenicol (50 μg/ml), to the broth.

Analysis of oligomerization

MCAD oligomerization was analyzed by SEC of the MBP–MCAD fusion proteins prior to cleavage with factor Xa. The MBP-tag increases solubility and yield during expression, but does not significantly affect the oligomeric state of the expressed proteins [own and previous observation (41)]. The size-exclusion column was calibrated using low molecular weight and high molecular weight gel filtration calibration kits (GE Healthcare). Blue dextran was used to determine the void volume (V_0, 46.0 ml).

Analyses of enzyme kinetic parameters

MCAD activity was determined using the ferricenium-based spectrophotometric assay described previously (42). Measurements were performed in 100 mM HEPES, pH 7.6, containing 0.1 mM EDTA at a temperature of 25°C with increasing concentrations of octanoyl-CoA (Sigma Aldrich, Larodan Chemicals) ranging from 0 to 20 μM (150 μM for the K_m variant). In order to correct for varying qualities of octanoyl-CoA with respect to the degree of purity, amount of crystal water and cationic ligands provided by the manufacturers, concentrations of oxidizable substrate were determined by complete turn-over using an excess of enzyme and electron acceptor. All measurements were corrected for background reduction of ferricenium.

The assays were performed in at least three independent experiments. The kinetic parameters K_m and V_{max} were averaged after non-linear regression analysis using the Michaelis–Menten algorithm implemented in pro Fit (QuantumSoft).

Limited proteolysis by proteinase K

Five micrograms of the purified tetrameric MCAD proteins were incubated with proteinase K (Sigma) using two different protease to substrate ratios, 1:1 and 1:25 by weight. The experiments were performed at 37°C in 20 mM HEPES buffer pH 7.0 containing 200 mM NaCl. Proteolysis was terminated at time points 2, 4, 6, 8, 10, 20, 30, 60 and 120 min by the addition of the inhibitor phenylmethylsulphonyl fluoride at a final concentration of 0.4 mM. The protein samples were subjected to SDS–PAGE under reducing conditions using 4–12% gradient polyacrylamide gels (Invitrogen). Proteolysis was monitored by Coomassie staining and subsequent densitometry analysis. Densitometry data were quantified by AIDA-software (Raytest), normalized to the intact MCAD protein prior to proteolysis and analyzed by non-linear regression. The experiments for each protease to substrate ratio were performed in triplicates. Significances for the differences between wild-type and variant proteins concerning plateau of proteolysis (protease to substrate ratio 1:1) and half-lives (protease to substrate ratio 1:25) were calculated using one-way ANOVA followed by a Dunnett's post test. Using the substrate ratio of 1:25 resulted in a slower decline of protein and, thus, was more suitable to determine half-lives.

Thermal inactivation experiments

To determine the effect of various temperatures on MCAD activity, aliquots of protein (5 μg/ml) were incubated in 100 mM HEPES, pH 7.6 containing 0.1 mM EDTA for 15 min at 11 different temperatures ranging from 25 to 55°C, and then chilled on ice. Enzyme activity was subsequently measured at an octanoyl-CoA concentration of 10 μM as described above. Residual activities were normalized to initial enzyme activity at 25°C.

For the assessment of thermal effects over time, one aliquot of protein (5 μg/ml) was incubated at 41°C with enzyme activities being determined at nine incremental time points (5–120 min). Residual activities were normalized to enzyme activity prior to incubation.

Data points were subjected to non-linear regression analysis and midpoints of thermal inactivation ($T_{1/2}$) and half-lives ($t_{1/2}$) were calculated; $T_{1/2}$ indicates the temperature and $t_{1/2}$ marks the time at 50% residual activity, respectively.

Measurements were performed in three independent experiments. Significances for the differences in $T_{1/2}$ and $t_{1/2}$ between wild-type and variant proteins were calculated using one-way ANOVA followed by a Dunnett's post test.

Thermal denaturation monitored by ANS fluorescence

Fluorescence measurements were performed on a Cary Eclipse fluorescence spectrophotometer equipped with a temperature-controlled Peltier multicell holder (Varian). Samples contained MCAD proteins (11.6 μM MCAD subunit) in 20 mM HEPES buffer at pH 7.0 containing 200 mM NaCl. The denaturation was monitored following the changes in ANS (purchased from Sigma) fluorescence emission: excitation at 395, emission at 450 nm (5.0/10.0 nm slit widths). The denaturation was performed at a rate of 1.2°C/min from 20 to 35°C and from 70 to 85°C and at a rate of 0.3°C/min from 35 to 70°C in three independent experiments. The transitions midpoints ($T_{m1/2}$), indicating the temperature at 50% denaturation, were calculated by the differentiation of the increasing part of the curves. Significances for the differences between wild-type and variants were calculated by one-way ANOVA and a Dunnett's post test.

Statistical analyses

Non-linear regression analyses and statistical tests were performed using GraphPad Prism 4.0c (GraphPad Software).

Structural analyses and figure preparation

The 3D structure of tetrameric pig MCAD complexed with the substrate analog 3-thiaoctanoyl-CoA (PDB code 1UDY) was analyzed using the DeepView-Swiss-PdbViewer (43). The porcine MCAD protein shows a >90% homology with human MCAD, and only homologous amino acid residues have been analyzed. In the presence of hydrogen atoms, H-bonds were computed with the following constraints: 1.2–2.76Å distance, 120° angles. When hydrogen atoms were absent, interactions were computed with the following

constraints: 2.35–3.2Å distance, 90° angles. Figures were prepared using VMD (44).

SUPPLEMENTARY MATERIAL

Supplementary Material is available at *HMG* online.

ACKNOWLEDGEMENTS

We are indebted to our patients and to their families; to Heike Preisler, Sylvia Taube and Sabine Streicher for excellent technical assistance; to Uta Nennstiel-Ratzel and Ralph Fingerhut for providing data on the biochemical phenotypes; to Mathias Woidy for helpful statistical discussions; to Jerry Vockley for providing the ACADM-encoding plasmid; to Dietrich Reinhardt for continuous support. This article is part of a thesis by J.M.J. and M.R. to fulfill the requirements for a medical degree at the Ludwig-Maximilians-University of Munich. This work was supported by the Bavarian Genome Research Network (BayGene); and the SHS International Gesellschaft für klinische Ernährung mbH.

Conflict of Interest statement. None declared.

FUNDING

Funding to pay the Open Access charge was provided by Bavarian Genome Research Network.

REFERENCES

1. Rhead, W.J. (2006) Newborn screening for medium-chain acyl-CoA dehydrogenase deficiency: a global perspective. *J. Inherit. Metab. Dis.*, **29**, 370–377.
2. Grosse, S.D., Khoury, M.J., Greene, C.L., Crider, K.S. and Pollitt, R.J. (2006) The epidemiology of medium chain acyl-CoA dehydrogenase deficiency: an update. *Genet. Med.*, **8**, 205–212.
3. Maier, E.M., Liebl, B., Röschinger, W., Nennstiel-Ratzel, U., Fingerhut, R., Olgemöller, B., Busch, U., Krone, N., von Kries, R. and Roscher, A.A. (2005) Population spectrum of *ACADM* genotypes correlated to biochemical phenotypes in newborn screening for medium-chain acyl-CoA dehydrogenase deficiency. *Hum. Mutat.*, **25**, 443–452.
4. Wilcken, B., Haas, M., Joy, P., Wiley, V., Chaplin, M., Black, C., Fletcher, J., McGill, J. and Boneh, A. (2007) Outcome of neonatal screening for medium-chain acyl-CoA dehydrogenase deficiency in Australia: a cohort study. *Lancet*, **369**, 37–42.
5. Derks, T.G., Reijngoud, D.J., Waterham, H.R., Gerver, W.J., van den Berg, M.P., Sauer, P.J. and Smit, G.P. (2006) The natural history of medium-chain acyl CoA dehydrogenase deficiency in the Netherlands: clinical presentation and outcome. *J. Pediatr.*, **148**, 665–670.
6. Iafolla, A.K., Thompson, R.J. Jr and Roe, C.R. (1994) Medium-chain acyl-coenzyme A dehydrogenase deficiency: clinical course in 120 affected children. *J. Pediatr.*, **124**, 409–415.
7. Wilcken, B., Hammond, J. and Silink, M. (1994) Morbidity and mortality in medium chain acyl coenzyme A dehydrogenase deficiency. *Arch. Dis. Child.*, **70**, 410–412.
8. Yokota, I., Indo, Y., Coates, P.M. and Tanaka, K. (1990) Molecular basis of medium chain acyl-coenzyme A dehydrogenase deficiency. An A to G transition at position 985 that causes a lysine-304 to glutamate substitution in the mature protein is the single prevalent mutation. *J. Clin. Invest.*, **86**, 1000–1003.
9. Gregersen, N., Andresen, B.S. and Bross, P. (2000) Prevalent mutations in fatty acid oxidation disorders: diagnostic considerations. *Eur. J. Pediatr.*, **159** (Suppl. 3), S213–S218.
10. Andresen, B.S., Bross, P., Udvari, S., Kirk, J., Gray, G., Kmoch, S., Chamoles, N., Knudsen, I., Winter, V., Wilcken, B. *et al.* (1997) The molecular basis of medium-chain acyl-CoA dehydrogenase (MCAD) deficiency in compound heterozygous patients: is there correlation between genotype and phenotype? *Hum. Mol. Genet.*, **6**, 695–707.
11. Bross, P., Andresen, B.S., Winter, V., Krautle, F., Jensen, T.G., Nandy, A., Kolvraa, S., Ghisla, S., Bolund, L. and Gregersen, N. (1993) Co-overexpression of bacterial GroESL chaperonins partly overcomes non-productive folding and tetramer assembly of *E.coli*-expressed human medium-chain acyl-CoA dehydrogenase (MCAD) carrying the prevalent disease-causing K304E mutation. *Biochim. Biophys. Acta*, **1182**, 264–274.
12. Bross, P., Jespersen, C., Jensen, T.G., Andresen, B.S., Kristensen, M.J., Winter, V., Nandy, A., Kräutle, F., Ghisla, S., Bolundi, L. *et al.* (1995) Effects of two mutations detected in medium chain acyl-CoA dehydrogenase (MCAD)-deficient patients on folding, oligomer assembly, and stability of MCAD enzyme. *J. Biol. Chem.*, **270**, 10284–10290.
13. Jensen, T.G., Bross, P., Andresen, B.S., Lund, T.B., Kristensen, T.J., Jensen, U.B., Winther, V., Kolvraa, S., Gregersen, N. and Bolund, L. (1995) Comparison between medium-chain acyl-CoA dehydrogenase mutant proteins overexpressed in bacterial and mammalian cells. *Hum. Mutat.*, **6**, 226–231.
14. Kieweg, V., Kräutle, F.G., Nandy, A., Engst, S., Vock, P., Abdel-Ghany, A.G., Bross, P., Gregersen, N., Rasched, I., Strauss, A. *et al.* (1997) Biochemical characterization of purified, human recombinant Lys304–>Glu medium-chain acyl-CoA dehydrogenase containing the common disease-causing mutation and comparison with the normal enzyme. *Eur. J. Biochem.*, **246**, 548–556.
15. Kuchler, B., Abdel-Ghany, A.G., Bross, P., Nandy, A., Rasched, I. and Ghisla, S. (1999) Biochemical characterization of a variant human medium-chain acyl-CoA dehydrogenase with a disease-associated mutation localized in the active site. *Biochem. J.*, **337**, 225–230.
16. Nasser, I., Mohsen, A.W., Jelesarov, I., Vockley, J., Macheroux, P. and Ghisla, S. (2004) Thermal unfolding of medium-chain acyl-CoA dehydrogenase and iso(3)valeryl-CoA dehydrogenase: study of the effect of genetic defects on enzyme stability. *Biochim. Biophys. Acta*, **1690**, 22–32.
17. Yokota, I., Saijo, T., Vockley, J. and Tanaka, K. (1992) Impaired tetramer assembly of variant medium-chain acyl-coenzyme A dehydrogenase with a glutamate or aspartate substitution for lysine 304 causing instability of the protein. *J. Biol. Chem.*, **267**, 26004–26010.
18. Andresen, B.S., Dobrowolski, S.F., O'Reilly, L., Muenzer, J., McCandless, S.E., Frazier, D.M., Udvari, S., Bross, P., Knudsen, I., Banas, R. *et al.* (2001) Medium-chain acyl-CoA dehydrogenase (MCAD) mutations identified by MS/MS-based prospective screening of newborns differ from those observed in patients with clinical symptoms: identification and characterization of a new, prevalent mutation that results in mild MCAD deficiency. *Am. J. Hum. Genet.*, **68**, 1408–1418.
19. Nichols, M.J., Saavedra-Matiz, C.A., Pass, K.A. and Caggana, M. (2008) Novel mutations causing medium chain acyl-CoA dehydrogenase deficiency: under-representation of the common c.985 A>G mutation in the New York state population. *Am. J. Med. Genet. A*, **146A**, 610–619.
20. Waddell, L., Wiley, V., Carpenter, K., Bennetts, B., Angel, L., Andresen, B.S. and Wilcken, B. (2006) Medium-chain acyl-CoA dehydrogenase deficiency: genotype-biochemical phenotype correlations. *Mol. Genet. Metab.*, **87**, 32–39.
21. O'Reilly, L., Bross, P., Corydon, T.J., Olpin, S.E., Hansen, J., Kenney, J.M., McCandless, S.E., Frazier, D.M., Winter, V., Gregersen, N. *et al.* (2004) The Y42H mutation in medium-chain acyl-CoA dehydrogenase, which is prevalent in babies identified by MS/MS-based newborn screening, is temperature sensitive. *Eur. J. Biochem.*, **271**, 4053–4063.
22. O'Reilly, L.P., Andresen, B.S. and Engel, P.C. (2005) Two novel variants of human medium chain acyl-CoA dehydrogenase (MCAD). K364R, a folding mutation, and R256T, a catalytic-site mutation resulting in a well-folded but totally inactive protein. *FEBS J.*, **272**, 4549–4557.
23. Kim, J.J. and Miura, R. (2004) Acyl-CoA dehydrogenases and acyl-CoA oxidases. Structural basis for mechanistic similarities and differences. *Eur. J. Biochem.*, **271**, 483–493.
24. Nandy, A., Kieweg, V., Kräutle, F.G., Vock, P., Kuchler, B., Bross, P., Kim, J.J., Rasched, I. and Ghisla, S. (1996) Medium-long-chain chimeric human Acyl-CoA dehydrogenase: medium-chain enzyme with the active center base arrangement of long-chain Acyl-CoA dehydrogenase. *Biochemistry*, **35**, 12402–12411.

25. Fontana, A., de Laureto, P.P., Spolaore, B., Frare, E., Picotti, P. and Zambonin, M. (2004) Probing protein structure by limited proteolysis. *Acta Biochim. Pol.*, **51**, 299–321.
26. Andresen, B.S., Bross, P., Jensen, T.G., Knudsen, I., Winter, V., Kolvraa, S., Bolund, L. and Gregersen, N. (1995) Molecular diagnosis and characterization of medium-chain acyl-CoA dehydrogenase deficiency. *Scand. J. Clin. Lab. Invest. Suppl.*, **220**, 9–25.
27. Royer, C.A. (1995) Fluorescence spectroscopy. *Methods Mol. Biol.*, **40**, 65–89.
28. Khoury, M.J., McCabe, L.L. and McCabe, E.R. (2003) Population screening in the age of genomic medicine. *N. Engl. J. Med.*, **348**, 50–58.
29. Gregersen, N., Bross, P., Andresen, B.S., Pedersen, C.B., Corydon, T.J. and Bolund, L. (2001) The role of chaperone-assisted folding and quality control in inborn errors of metabolism: protein folding disorders. *J. Inherit. Metab. Dis.*, **24**, 189–212.
30. Yang, B.Z., Ding, J.H., Zhou, C., Dimachkie, M.M., Sweetman, L., Dasouki, M.J., Wilkinson, J. and Roe, C.R. (2000) Identification of a novel mutation in patients with medium-chain acyl-CoA dehydrogenase deficiency. *Mol. Genet. Metab.*, **69**, 259–262.
31. Toogood, H.S., Leys, D. and Scrutton, N.S. (2007) Dynamics driving function: new insights from electron transferring flavoproteins and partner complexes. *FEBS J.*, **274**, 5481–5504.
32. Volchenboum, S.L., Mohsen, A.W., Kim, J.J. and Vockley, J. (2001) Arginine 387 of human isovaleryl-CoA dehydrogenase plays a crucial role in substrate/product binding. *Mol. Genet. Metab.*, **74**, 226–237.
33. Fu, Z., Wang, M., Paschke, R., Rao, K.S., Frerman, F.E. and Kim, J.J. (2004) Crystal structures of human glutaryl-CoA dehydrogenase with and without an alternate substrate: structural bases of dehydrogenation and decarboxylation reactions. *Biochemistry*, **43**, 9674–9684.
34. Saijo, T. and Tanaka, K. (1995) Isoalloxazine ring of FAD is required for the formation of the core in the Hsp60-assisted folding of medium chain acyl-CoA dehydrogenase subunit into the assembly competent conformation in mitochondria. *J. Biol. Chem.*, **270**, 1899–1907.
35. Gregersen, N., Andresen, B.S., Pedersen, C.B., Olsen, R.K., Corydon, T.J. and Bross, P. (2008) Mitochondrial fatty acid oxidation defects–remaining challenges. *J. Inherit. Metab. Dis.*, **31**, 643–657.
36. Gersting, S.W., Kemter, K.F., Staudigl, M., Messing, D.D., Danecka, M.K., Lagler, F.B., Sommerhoff, C.P., Roscher, A.A. and Muntau, A.C. (2008) Loss of function in phenylketonuria is caused by impaired molecular motions and conformational instability. *Am. J. Hum. Genet.*, **83**, 5–17.
37. Levy, H.L., Milanowski, A., Chakrapani, A., Cleary, M., Lee, P., Trefz, F.K., Whitley, C.B., Feillet, F., Feigenbaum, A.S., Bebchuk, J.D. *et al.* (2007) Efficacy of sapropterin dihydrochloride (tetrahydrobiopterin, 6R-BH4) for reduction of phenylalanine concentration in patients with phenylketonuria: a phase III randomised placebo-controlled study. *Lancet*, **370**, 504–510.
38. Muntau, A.C., Röschinger, W., Habich, M., Demmelmair, H., Hoffmann, B., Sommerhoff, C.P. and Roscher, A.A. (2002) Tetrahydrobiopterin as an alternative treatment for mild phenylketonuria. *N. Engl. J. Med.*, **347**, 2122–2132.
39. Mu, T.W., Ong, D.S., Wang, Y.J., Balch, W.E., Yates, J.R. III, Segatori, L. and Kelly, J.W. (2008) Chemical and biological approaches synergize to ameliorate protein-folding diseases. *Cell*, **134**, 769–781.
40. Goloubinoff, P., Gatenby, A.A. and Lorimer, G.H. (1989) GroE heat-shock proteins promote assembly of foreign prokaryotic ribulose bisphosphate carboxylase oligomers in *Escherichia coli*. *Nature*, **337**, 44–47.
41. Kapust, R.B. and Waugh, D.S. (1999) *Escherichia coli* maltose-binding protein is uncommonly effective at promoting the solubility of polypeptides to which it is fused. *Protein Sci.*, **8**, 1668–1674.
42. Lehman, T.C., Hale, D.E., Bhala, A. and Thorpe, C. (1990) An acyl-coenzyme A dehydrogenase assay utilizing the ferricenium ion. *Anal. Biochem.*, **186**, 280–284.
43. Satoh, A., Nakajima, Y., Miyahara, I., Hirotsu, K., Tanaka, T., Nishina, Y., Shiga, K., Tamaoki, H., Setoyama, C. and Miura, R. (2003) Structure of the transition state analog of medium-chain acyl-CoA dehydrogenase. Crystallographic and molecular orbital studies on the charge-transfer complex of medium-chain acyl-CoA dehydrogenase with 3-thiaoctanoyl-CoA. *J. Biochem.*, **134**, 297–304.
44. Humphrey, W., Dalke, A. and Schulten, K. (1996) VMD: visual molecular dynamics. *J. Mol. Graph.*, **14** (33–38), 27–38.